Estimation of Dynamically Evolving Ellipsoids with Applications to Medical Imaging

Seema Jaggi, *Student Member, IEEE,* William C. Karl, *Member, IEEE,* and Alan S. Willsky, *Fellow, IEEE*

Abstract— **The estimation of dynamically evolving ellipsoids from noisy lower-dimensional projections is examined. In particular, this work describes a model-based approach using geometric reconstruction and recursive estimation techniques to obtain a dynamic estimate of left-ventricular ejection fraction from a gated set of planar myocardial perfusion images. The proposed approach differs from current ejection fraction estimation techniques both in the imaging modality used and in the subsequent processing which yields a dynamic ejection fraction estimate. For this work, the left ventricle is modeled as a dynamically evolving three-dimensional (3-D) ellipsoid. The left-ventricular outline observed in the myocardial perfusion images is then modeled as a dynamic, two-dimensional (2-D) ellipsoid, obtained as the projection of the former 3-D ellipsoid. This data is processed in two ways: first, as a 3-D dynamic ellipsoid reconstruction problem; second, each view is considered as a 2-D dynamic ellipse estimation problem and then the 3-D ejection fraction is obtained by combining the effective 2-D ejection fractions of each view. The approximating ellipsoids are reconstructed using a Rauch-Tung-Striebel smoothing filter, which produces an ejection fraction estimate that is more robust to noise since it is based on the *entire* data set; in contrast, traditional ejection fraction estimates are based *only on two frames* of data. Further, numerical studies of the sensitivity of this approach to unknown dynamics and projection geometry are presented, providing a rational basis for specifying system parameters. This investigation includes estimation of ejection fraction from both simulated and real data.**

I. Introduction

THIS RESEARCH presents a medical imaging application of the estimation of dynamically evolving ellipsoids from noisy projection observations. Much work in geometric reconstruction [1]–[5] has focused on reconstructing objects such as ellipsoids from noisy lower-dimensional projections. This work differs from previous applications of ellipsoid reconstruction [3] since the precise ellipsoid dynamics and projection geometries are unknown. In particular, a method to obtain the ejection fraction of the left ventricle of the heart from a gated set of planar radionuclide (^{99m}Tc) myocardial perfusion images [6]–[8] is presented. Gated myocardial perfusion imaging is a radionuclide technique that may be used to produce a sequential set of images of the heart in motion, which are not traditionally used to estimate ejection fraction. The model-based approach described in this paper employs geometric reconstruction and recursive estimation techniques to track left ventricular shape throughout the cardiac cycle. This approach allows the generation of a *dynamically based* ejection fraction estimate, which we show is more robust to variations due to noise than traditional *static* ejection fraction estimates. Our proposed approach differs from current ejection fraction estimation techniques, both in the imaging modality used and in the subsequent processing which yields a dynamic ejection fraction estimate.

The ejection fraction (EF) of the left ventricle has long been known as an effective gauge of cardiac function [9] and has great prognostic value to cardiologists. The ejection fraction is defined as

$$\mathrm{EF} = 1 - \frac{\text{end systolic volume}}{\text{end diastolic volume}} \tag{1}$$

where end systole (ES) and end diastole (ED) are the fully contracted and fully expanded cardiac phases, respectively.

In this work, a temporal set of planar myocardial perfusion images [6]–[8] is used to estimate ejection fraction. Traditionally, these images are not used to estimate ejection fraction. These observations are obtained by injecting the patient with a radionuclide marked substance (^{99m}Tc in this case) and imaging with a gamma camera. Sixteen images are produced at equally spaced points in the cardiac cycle via ECG-gating. The resulting images are the sum of a particular cardiac phase over many cardiac cycles, not snapshots of the heart in motion. The data set consists of images from three views: anterior (ANT), lateral (LAT), and left anterior oblique (LAO). ANT is a frontal view; LAT is a side view, underneath the left arm; and LAO is a frontal view, skewed down and to the left side (see Fig. 1). This data-acquisition modality coupled with beat-to-beat variability combine to give poor visual quality images.

Myocardial perfusion images, while of poor visual quality, contain a large amount of *physiological* information reflecting the tie between the chosen radionuclide and the biochemistry of the region under study. As a result, these images are traditionally used to locate infarcts, areas in the heart muscle that are being deprived of nutrients because of an occlusion in the vessels of the heart. In addition to this traditional role, it is possible to distinguish the outline of the left ventricular chamber from myocardial perfusion images and to obtain *structural* information about the left ventricle. In this work,

Manuscript received September 1, 1993; revised January 16, 1995. This work was supported in part by the National Science Foundation under Grant 9015281-MIP, Army Research Office under Grant DAAL03-92-G-0115, and the Office of Naval Research under Grant N00014-91-J-1004. The Associate Editor responsible for coordinating the review of this paper and recommending its publication was R. Leahy.

S. Jaggi and A. S. Willsky are with the Laboratory for Information and Decision Systems, Massachusetts Institute of Technology, Cambridge, MA 02139 USA; e-mail: jaggi@mit.edu.

W. C. Karl is with the Department of Electrical, Computer and Systems Engineering, Boston University, Boston, MA 02215 USA.

IEEE Log Number 9411365.

Fig. 1. A sample ANT myocardial perfusion image. The horseshoe-shaped object in the center is the left ventricular wall.

we will estimate the ejection fraction from this projection-like outline of the left ventricle.

Geometric reconstruction and recursive estimation techniques are used here to formulate a dynamically based ejection fraction estimate which is more robust to variations due to noise than traditional static ejection fraction estimates. One commonly used approximation to the true shape of the left ventricle is a 3-D ellipsoid [10]–[12]. The projections (or shadows) of this left ventricular ellipsoidal model are 2-D ellipsoids which model the left ventricular outline in the observed myocardial perfusion images. By projections, we mean shadow projections of this ellipsoidal shape as opposed to line integral projections. By combining previous work in geometric reconstruction [3] with a statistical recursive estimation procedure known as Rauch-Tung-Striebel (RTS) smoothing [13], it is possible to formulate an efficient estimation procedure that combines the observed temporal set of projection images with an evolution model to produce the estimate of the ellipsoid which minimizes mean-square error at any point given all the data. This smoothing technique combines *all the frames* of data to estimate the left ventricular volume at ES and ED. This dynamically based ejection fraction estimate is more robust to noise compared to traditional techniques, where the ejection fraction estimate is calculated from volume estimates at ES and ED based on *only those two frames* of data.

We examine two ways of processing the projection data. In the first, the three projection views are processed together as a single 3-D ellipsoid reconstruction problem. In the second, simpler method, each view is processed individually as a 2-D dynamic ellipse estimation problem; the 3-D ejection fraction estimate is calculated by combining the effective 2-D ejection fractions obtained from each view.

Many techniques exist for estimating ejection fraction including angiography [10], echocardiography [14], magnetic resonance imaging [15], and radionuclide ventriculography [10], [16]. The "gold standard" (GS) estimate of ejection fraction used here is based on multiple-gated blood pool (MUGA) images. The ultimate objective of this work will be to show a high degree of correlation between our ejection fraction estimates based on myocardial perfusion images and standard estimates based on MUGA.

Several important points should be noted in comparing our ejection fraction estimates based on myocardial perfusion images to those based on MUGA. First, an ejection fraction estimate based on myocardial perfusion images provides a safer and more cost-effective alternative to the MUGA based estimates. This is because the typical diagnostic procedure includes both myocardial perfusion imaging to obtain physiological information about possible cardiac infarcts and MUGA imaging to estimate ejection fraction. Thus, by estimating ejection fraction from myocardial perfusion images alone, we may be able to eliminate the need for MUGA imaging and minimize the patient's exposure to radiation. Second, the smoothing techniques combine *all the frames* of data (in contrast to current techniques) to give an ejection fraction estimate which is more robust to variations due to noise. Third, in a formulation based on geometric reconstruction and statistical methods, the modeling assumptions are explicitly stated. Thus, it is possible to investigate the sensitivity of the estimate with respect to these assumptions. Indeed, we do precisely that in Section III.

The dynamically based smoothing techniques presented in this work are also directly applicable to ejection fraction estimates from other imaging modalities. That is, similar smoothing filter-based reconstruction could be applied to MUGA images or even angiographic data. Again, our dynamically based smoothing techniques combine the entire data set to give an ejection fraction estimate which is more robust to variations due to noise than those methods using only two frames of data.

The organization of this paper is as follows. In Section II, the necessary background from geometric reconstruction and statistical recursive estimation is discussed together with their application to the estimation of ejection fraction from myocardial perfusion images. In Sections III and IV, we test our methods on simulated and real myocardial perfusion data, respectively.

II. Problem Formulation

This section summarizes the mathematical background needed to describe the reconstruction of an n-dimensional dynamically evolving ellipsoid and the application of ellipsoid reconstruction to the processing of myocardial perfusion images to estimate ejection fraction.

A. Mathematical Background

Consider the general problem of reconstructing a dynamically evolving n-dimensional ellipsoid from a series of noisy (perhaps lower-dimensional projection) observations [3]. This problem may be greatly simplified by choosing appropriate representations for the ellipsoids, their dynamics, and their projections. Several such representations (including the one used in this work) are discussed in [3]. It is possible to

represent the points included in an n-dimensional, origin-centered nondegenerate ellipsoid in the following way:

$$\{z \mid z^T X^{-1} z \leq 1, z \in R^n\} \tag{2}$$

where the symmetric, positive definite $n \times n$ matrix X that represents the ellipsoid is easily determined. For example, a 2-D ellipsoid (an ellipse) centered at the origin with semiaxis lengths, a and b, and an angle of rotation ϕ is represented by the matrix

$$X = \begin{pmatrix} \cos\phi & \sin\phi \\ -\sin\phi & \cos\phi \end{pmatrix}^T \begin{pmatrix} a^2 & 0 \\ 0 & b^2 \end{pmatrix} \begin{pmatrix} \cos\phi & \sin\phi \\ -\sin\phi & \cos\phi \end{pmatrix}.$$

The projections of an ellipsoid are themselves ellipsoids of lower dimension. The symmetric matrix representation of the ellipsoid in (2) yields a linear relationship between the matrix X that represents the ellipsoid and the matrix Y_i that represents the ellipsoid in a given projection. In particular, this relationship is given by

$$Y_i = C_i^T X C_i \tag{3}$$

where the columns of C_i span the space of the projection, capturing the projection geometry.

By representing an ellipsoid by its associated matrix X, it is possible to capture a broad range of ellipsoid dynamics through the following evolution equation:

$$X(k+1) = A(k)^T X(k) A(k) \tag{4}$$

where changes such as magnification, rotation, and eccentricity change may be included in a simple way in $A(k)$. For example, in the 2-D case, one convenient choice for $A(k)$ is (see [5])

$$A(k) = c(k) \begin{pmatrix} \alpha(k) & 0 \\ 0 & 1/\alpha(k) \end{pmatrix} \begin{pmatrix} \cos\theta(k) & \sin\theta(k) \\ -\sin\theta(k) & \cos\theta(k) \end{pmatrix} \tag{5}$$

where the first term represents uniform scaling by the factor $c(k) \geq 0$, the second term an area preserving stretching along the coordinate axes by $\alpha(k) \geq 0$, and the last term a rotation by an angle $\theta(k)$. This general form is easily extended to express similar dynamics for ellipsoids of higher dimensions.

Now, if we have *noisy* observations of the evolving matrix $X(k)$ of the form (3), these may be captured by the observation equation

$$Y_i(k) = C_i^T X(k) C_i + V_i(k) \tag{6}$$

where the symmetric matrix $V_i(k)$ represents the effects of observation noise. Note that this model assumes that our observations are actually *ellipsoids*, with the uncertainty appearing in the exact shape of the ellipsoid. To simplify the ellipsoid reconstruction problem, we assume that the independent elements of $V_i(k)$ have a Gaussian distribution.[1]

By casting the geometrically intuitive formulas (4) and (6) in standard state space form, it is possible to invoke the well-developed methods of recursive estimation theory and still preserve the geometric interpretation of the original problem formulation. Note that the set of $n \times n$ symmetric matrices forms a $\frac{n(n+1)}{2}$-dimensional vector space. Thus, there exists an *equivalent* vector representation for the linear ellipsoid dynamics (4) and the observation equation (6) given by

$$x(k+1) = \tilde{A}(k) x(k) \tag{7}$$

$$y(k) = \tilde{C} x(k) + v(k) \tag{8}$$

where the matrices $\tilde{A}$ and $\tilde{C}$ are matrix representations of the linear operators on $X(k)$ defined in (4) and (6) with respect to given orthonormal bases on the sets of symmetric matrices of corresponding dimension. Thus, there is a one-to-one correspondence between $X(k)$ and $x(k)$ (similarly between $Y(k)$ and $y(k)$) and our intuition about the ellipsoid evolution and measurement equations is preserved. In [3], specific orthonormal bases for the matrices $\tilde{A}$ and $\tilde{C}$ are discussed. Specifically, the matrix $\tilde{C}$ is obtained by stacking the matrix representations of each of the linear operators $(C_i^T(\cdot)C_i)$. Further, it follows from (6) that the term $v(k)$ is a Gaussian vector with zero mean and variance $R = rI$. This problem formulation is directly amenable to the extensive set of techniques from recursive estimation. In particular, the Rauch-Tung-Striebel (RTS) smoothing algorithm [13] may be used to obtain $\hat{x}(k \mid T)$, the estimate of the ellipsoid $x(k)$ at time k which minimizes mean-square error given data over $[0, T]$.

B. Application to Processing of Myocardial Images

A few comments are in order before we proceed. Recall that the formulation of (6) assumes that our observations are ellipsoids (albeit perturbed ones) and not images. Since this is not the focus of this paper, we assume that a preprocessing step which extracts ellipses and provides the statistics of the measurement noise is available. There exist many such methods to extract both ellipses from planar data and the statistics of $v(k)$ in (8) [17]–[19]. In addition, note that the transformation from the ellipsoid shape, as specified by the symmetric matrix $X(k)$ (or equivalently by $x(k)$), to the ejection fraction is a nonlinear one and that the transformation between ellipses and ejection fraction is not one-to-one since many combinations of different maximum and minimum ellipses will yield the same ejection fraction.

In this section, we use the formulation in Section II-A to combine the information in the different projection views in two ways. The first approach is to process the three projection views together in a single 3-D ellipsoid reconstruction problem, i.e., our observations are taken to be 2-D projections of an underlying 3-D ellipsoid. An ejection fraction estimate is then based on the resulting reconstructed 3-D dynamic ellipsoid according to (1). Of course, this approach inherently requires that a projection geometry be specified which we describe later in this section.

An alternative, simpler method is to process each lower-dimensional view individually as an independent 2-D ellipse estimation problem; hence, three 2-D dynamic ellipse estimates are obtained. In this case, our observations are of the 2-D ellipses themselves. For each of these three dynamic ellipse estimates, a corresponding apparent planar "ejection fraction"

[1] This model is not strictly proper since it implies that $Y_i(k)$ will not always be a positive definite matrix, which it must be to represent an ellipsoid. However, we choose to employ this commonly used assumption because of the simplification it provides in the ellipsoid reconstruction problem.

can be found. The overall ejection fraction may then be obtained by combining these 2-D ejection fractions calculated from each view under certain simplifying assumptions. For example, by assuming the projection views onto three mutually orthogonal planes aligned with the ellipsoid axes, the ejection fraction of the 3-D ellipsoid is given by

$$\mathrm{EF} = 1 - \sqrt{(1 - \mathrm{EF}_{\mathrm{view1}})(1 - \mathrm{EF}_{\mathrm{view2}})(1 - \mathrm{EF}_{\mathrm{view3}})} \tag{9}$$

where EF is the overall ejection fraction of the 3-D ellipsoid and $\mathrm{EF}_{\mathrm{view}i}$ is the apparent ejection fraction of the ellipses in projection i. Note that this formulation implicitly assumes a projection geometry, i.e., orthogonal projections onto planes aligned with the ellipsoid axes.

Regardless of how we use the results of Section II-A to combine the data, two significant obstacles must be addressed to obtain reliable ejection fraction estimates from the real data. First, obviously, the dynamics of the ellipsoid which approximates the left ventricle are unknown and vary from person to person. Thus, the underlying ellipsoid dynamics, as captured by $A(k)$, are unknown to us (though we clearly have significant prior knowledge in this regard). Second, the gamma camera is positioned to obtain roughly the ANT, LAT, and LAO views, but the exact position varies from patient to patient. Therefore, the projection geometry, as captured explicitly in C or implicitly in a formulation such as (9) is imperfectly known.

1) Imperfectly Known Dynamics: In this work, we use a model identification scheme based on hypothesis testing to determine a coarse approximation to the true ellipsoid dynamics. The RTS smoothing filter reconstruction is then based on the dynamics chosen by the model identification scheme. Note that because the model identification yields only a coarse approximation to the true dynamics, model mismatch will still remain in the smoothing filter reconstruction. We discuss how to account for this effect later in this section.

Given our significant prior knowledge of cardiac dynamics, it is straightforward to define a small set of reasonable hypothesized dynamic models. In particular, we assume that the underlying left ventricular dynamics correspond to a uniform shrinking phase followed by a uniform expansion phase, the only uncertainty being in the rate. Each hypothesized model is thus based on a hypothesized rate parameter which induces an associated ejection fraction. Since it is ejection fraction that is of interest to us and each model has associated with it a corresponding (unique) ejection fraction, we will often refer to these different models by their associated ejection fractions.

Model identification is a stochastic estimation technique which determines which of several hypothesized models is most likely given the data. That is, the model identifier chooses model i from m hypothesized models at time k if model i maximizes the quantity

$$p_i(k) = \Pr(\text{model } i \text{ is correct} \mid \mathcal{Y}_k) \tag{10}$$

where $\mathcal{Y}_k$ is the set of measurements up to and including the measurement at time k. Applying Bayes' rule, $p_i(k)$ is given by the following recursive form:

$$\frac{p(y(k) \mid \mathcal{Y}_{k-1},\ \text{model } i \text{ is correct}) p_i(k-1)}{\sum_{j=1}^{m} p(y(k) \mid \mathcal{Y}_{k-1},\ \text{model } j \text{ is correct}) p_j(k-1)}. \tag{11}$$

The quantity $p(y(k) \mid \mathcal{Y}_{k-1}, \text{model } i \text{ is correct})$ is obtained as a byproduct of the Kalman filter based on model i and is given by

$$p(y(k) \mid \mathcal{Y}_{k-1}, \text{model } i \text{ is correct}) = N(\nu_i(k); 0, \mathcal{V}_i(k)) \tag{12}$$

where $N(\nu_i(k); 0, \mathcal{V}_i(k))$ is a Gaussian distribution with a mean of zero and a variance $\mathcal{V}_i(k)$ evaluated at $\nu_i(k)$, the Kalman filter residuals at time k under hypothesis i. Both $\nu_i(k)$ and $\mathcal{V}_i(k)$ are obtained directly from the Kalman filter. By substituting (12) in (11), we can evaluate $p_i(k)$. Thus, the model identification scheme consists of a bank of Kalman filters, one based on each of the hypothesized models, and a comparison step to determine which hypothesized model maximizes $p_i(T)$, where T is the time interval over which we have collected data.

Since the model identification phase yields only a coarse approximation to the true dynamics, a residual dynamic model mismatch will still remain in the smoothing filter-based ejection fraction estimates. One method to compensate for this remaining error is through the addition of a process noise term to the modeled dynamics in (7) on which we will base our filter; that is, the error introduced by dynamic model mismatch is modeled as a process noise with a variance of $Q = qI$. In general, the smoothed state estimate at any time is a weighted average of the measured and predicted states. In the smoothing filter, the variance of such a process noise term may be interpreted as a measure of the trust in the dynamic model, and thus the predicted state versus the measured data. If q is very high, the estimate will be based on the measurements alone. In contrast, if q is low, the estimate will be based on the predicted state (and thus the dynamic model and initial condition) alone. Hence, the value of q may be used to compensate for the effect of dynamic model mismatch by reducing the dependence on the model in the estimate.

2) Imperfectly Known Projection Geometry: Beyond imperfect knowledge of the ellipsoid dynamics, the relationship between the ellipsoid and our projection observations of it, i.e., the projection geometry specified by C_i, is imperfectly known. For this work, we will simply assume orientations for the three projection planes then examine the sensitivity of our reconstructions to this assumption.[2]

We expect that the effect of errors in this assumed projection geometry on the resulting *ejection fraction* estimate to be minimal for the following reasons. First, the left ventricle is a minimally eccentric ellipsoid; its shape tends toward a sphere. Thus, the assumed projection geometry introduces minimal error in the ejection fraction estimate. Second, the dynamics of the left ventricle include only a slight rotation. For the simple case where the dynamics consist of only isotropic contraction without rotation, it is easy to show that the assumed projection

[2] One could also imagine developing a further hypothesis testing procedure to estimate the projection geometry.

geometry does not introduce *any* error into the ejection fraction estimate. Even for more complicated dynamics, which include isotropic contraction and a gross rotation, the effect of the assumed projection geometry on the ejection fraction estimate is minimal.

3) 3-D Versus 2-D Processing: For the 3-D processing, the three views are processed together as a single 3-D model identification/reconstruction problem. That is, the model identifier and smoothing filter-based reconstruction are used to reconstruct the 3-D ellipsoid that best approximates the left ventricle based on the set of noisy 2-D projections in the three views. The outcome of the model identifier is used to provide a dynamic model for the smoothing filter-based reconstruction. Based on the volume of the estimated 3-D ellipsoids which are the output of the smoothing filter, an estimate of the ejection fraction is calculated according to (1). Since the true projection geometry is unknown, we use an assumed projection geometry that approximates the standard ANT, LAT, and LAO views. In particular, we assume our three projections are onto the xz-plane, the yz-plane, and a plane which is tilted at an angle $\Theta = 45°$ from the xy-plane, as shown in Fig. 2. This third plane is completely specified by its normal, p_n, where

$$p_n = (-\cos\Phi\sin\Theta, -\sin\Phi\sin\Theta, \cos\Theta). \tag{13}$$

This assumed (or modeled) projection geometry is captured in (6) by the set of matrices

$$C_{m1} = \begin{pmatrix} 1 & 0 & 0 \\ 0 & 1 & 0 \end{pmatrix} \tag{14}$$

$$C_{m2} = \begin{pmatrix} 0 & 1 & 0 \\ 0 & 0 & 1 \end{pmatrix} \tag{15}$$

$$C_{m3} = \begin{pmatrix} -\sin\Phi & \cos\Phi & 0 \\ \cos\Phi\cos\Theta & \sin\Phi\cos\Theta & \sin\Theta \end{pmatrix}. \tag{16}$$

Equivalently, the assumed projection geometry may be represented by $\tilde{C}_m$, obtained by stacking the matrix representations of the linear operators C_{mi}, as discussed in Section II-A.

Our alternative method of combining the three views of data to estimate the ejection fraction is to process each view individually as a 2-D problem. That is, we use a model identifier to individually estimate the dynamics of the ellipses observed in each view. The outcome of the model identifier is then used to provide a dynamic model for the smoothing filter-based reconstruction of the ellipse trajectory in that view. Based on the smoothed ellipses, the apparent 2-D "ejection fraction" for each view is calculated. For 2-D processing, the matrix $\tilde{C}$ in (8), which relates the ellipsoid to the measurements, is given by the identity. Note that each 2-D ejection fraction actually underestimates the underlying 3-D ejection fraction. The overall ejection fraction estimate is then formulated using the formula given in (9).

III. Simulations

In this section, we present simulation results which illustrate the methods outlined in Section II. Included are simulations to investigate the performance of the model identifier, the effect of the dynamic model mismatch, and the sensitivity to the assumed projection geometries.

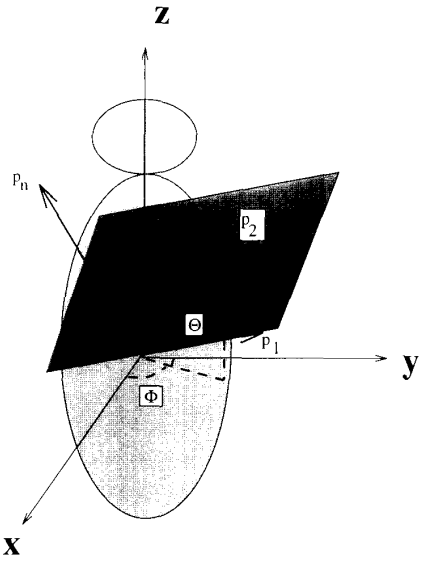

Fig. 2. Projection plane orientation.

A. Model Identification

Two experiments were conducted to evaluate the performance of the model identifier. For both Experiment #1 and #2, the following simulation setup is assumed. A computer-simulated 3-D ellipsoid and its projection measurements are generated as described by (7) and (8). The initial ellipsoid has semiaxis lengths of 8, 7.2, and 8, aligned with the x-, y-, and z-axes, respectively. The true dynamics are expressed by matrices $A_t(k)$ of the form

$$A_t(k) = \begin{cases} c_t\mathcal{R}(\theta_t) & \text{for } (1 \le k \bmod 16 + 1) \le 8 \\ 1/c_t\mathcal{R}(-\theta_t) & \text{for } (9 \le k \bmod 16 + 1) \le 16 \end{cases} \tag{17}$$

where $\mathcal{R}(\cdot)$ describes rotation about the x-axis and is a generalization of the last term in (5); c_t and θ_t are the true rates of contraction and rotation, respectively. These true dynamics generate a shrinking/rotating and expanding/rotating ellipsoid. Since the myocardial perfusion data consists of 16 frames per cycle, the simulated ellipsoid cycle was chosen to be 16. The ejection fraction that corresponds to the true model (17) will be denoted EF_t. The measurements, as described by (3), are taken to be noisy projections onto three orthogonal planes which are aligned with the ellipsoid axes. This projection geometry corresponds to projections on the xy-, yz-, and xz-planes and is represented by C_1, C_2, C_3 in (14)–(16) with $\Phi = \Theta = 0$, or equivalently, by the matrix $\tilde{C}$, as described in Section II-A.

The model identifier is based on two hypothesized dynamical models with associated dynamic matrices A_1 and A_2. These hypothesized dynamics have corresponding contraction rates of c_1 and c_2 and rotation rates of θ_1 and θ_2. The matrices A_1 and A_2 are of the same form as (17) with true contraction and rotation rates replaced by the corresponding modeled contraction and rotation rates. The ejection fractions corresponding to the two hypothesized models, A_1 and A_2,

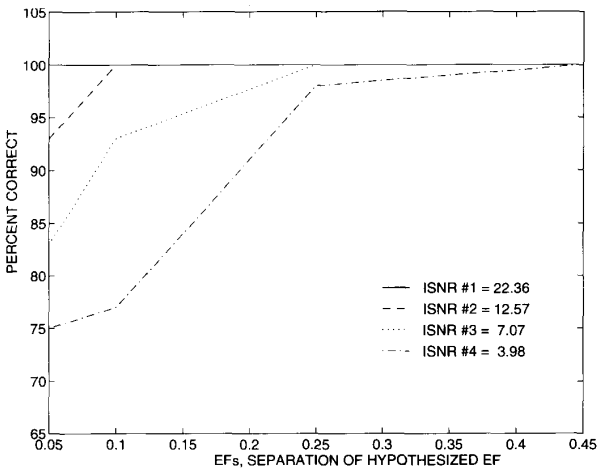

Fig. 3. Model identification Experiment #1 results.

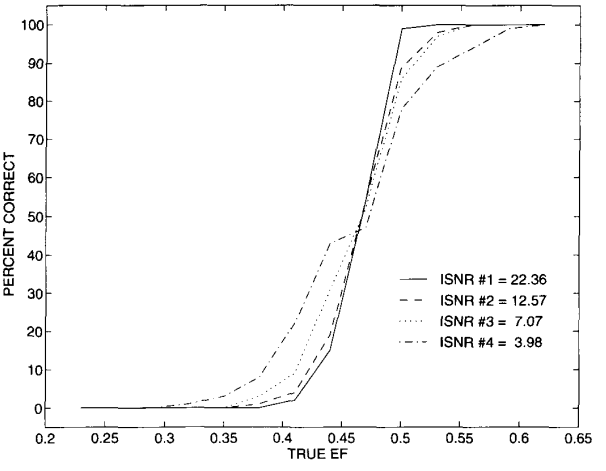

Fig. 4. Model identification Experiment #2 results.

will be denoted as EF_1 and EF_2. Experiments #1 and #2 differ in which of the values c_t, c_1, c_2, θ_t, θ_1, and θ_2 are held fixed and which are varied. The model identifier is initialized with the linear least squares estimate of the ellipse at time $k = 0$ and with an initial error covariance, P_0, which is high to indicate that our confidence in this initial estimate is low. Our initialization is given in (18) and (19) where $R = rI$ is the measurement noise variance.

$$\hat{x}(1 \mid 0) = (\tilde{C}^T\tilde{C})^{-1}\tilde{C}^T y(1) \tag{18}$$

$$P_0 = 5R. \tag{19}$$

Both sets of experiments will be carried out for several levels of measurement noise variance. This noise variance will be held constant throughout the experiment interval. We will categorize each noise level by the initial signal-to-noise ratio (ISNR) defined as

$$\mathrm{ISNR} = \sqrt{\frac{\|x(1)\|^2}{nr}} \tag{20}$$

where $x(1)$ is the vector representation of the ellipsoid at time $k = 1$, n is the dimension of x, and r is the variance of the measurement noise. The ISNR for each of the four measurement noise levels under consideration are listed in the legend of Fig. 3. The noise levels are chosen to cover the range of variability expected from typical ellipse extraction routines.

The objective of Experiment set #1 is to investigate how sensitive the model identifier is to the separation of the hypothesized ejection fractions when one of the hypothesized dynamic models exactly matches the dynamics used to create the set of ellipses. Even though such a scenario does not exist in the real world, this exercise is useful since it illustrates the sensitivity performance of the model identification scheme. In Experiment set #1, the true dynamics and ejection fraction always equal those associated with hypothesized Model #1 (i.e., $c_t = c_1$, $\mathrm{EF}_t = \mathrm{EF}_1$) and c_2 is allowed to vary. For Experiment set #1, neither the true nor modeled dynamics include rotation (i.e., $\theta_t = \theta_1 = \theta_2 = 0$). The hypothesized models have associated ejection fractions that yield an EF separation which is given by $\mathrm{EF}_s = \mathrm{EF}_1 - \mathrm{EF}_2 = \mathrm{EF}_t - \mathrm{EF}_2$. The performance of the model identifier is evaluated at four ISNR levels as EF_s is decreased. To control the complexity of this experiment, the projection geometry was assumed known to the model identifier. Fig. 3 shows the number of realizations out of 100 that correctly identify Model #1 as a function of the separation between the two hypothesized ejection fractions and the measurement noise level. These results indicate that for high ISNR the model identifier always chooses the correct model regardless of the separation between the two hypothesized ejection fractions. Although the performance deteriorates for lower ISNR levels, these results indicate that 75% correct identification can be obtained over an extremely wide range of separations even for low ISNR levels.

The objective of Experiment set #2 is to evaluate the performance of the model identification scheme when the true ellipsoid dynamics include contraction, expansion, and rotation, but the hypothesized models are simpler, including only contraction and expansion at a rate that differs from the true contraction/expansion for a wide range of ISNR levels. To study this case, the dynamics and thus, ejection fractions of the two hypothesized models are fixed and the true dynamics vary so that the true ejection fraction varies between those of the two hypothesized models. The two hypothesized dynamic models are captured by dynamic matrices A_1 and A_2 of the form (17) with hypothesized contraction rates of $c_1 = 0.9572$ and $c_2 = 0.9907$ which correspond to ejection fractions of $\mathrm{EF}_1 = 0.65$ and $\mathrm{EF}_2 = 0.20$. These modeled dynamics do not include rotation (i.e., $\theta_1 = \theta_2 = 0$). The true ellipsoid dynamics are also of the form (17) with values of c_t in the range from 0.9605 to 0.9892, which correspond to values of EF_t from 0.62 down to 0.23. The true dynamics include a rotation at each step of $\theta_t = \pi/54$ about the x-axis, which implies a total rotation of $\pi/6$. Fig. 4 shows the number of realizations out of 100 that picked Model #1 given all the data for each value of c_t. For ISNR #1, the model identifier performs as follows: If $\mathrm{EF}_t \gtrsim 0.47$, then Model #1 is chosen; if $\mathrm{EF}_t \lesssim 0.4$, then Model #2 is chosen; if $0.4 \lesssim \mathrm{EF}_t \lesssim 0.47$,

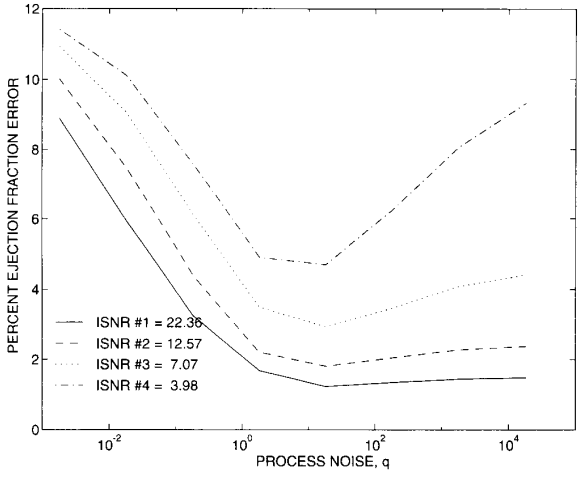

Fig. 5. Ejection fraction error using an assumed dynamic model.

	Semi-Axis Lengths	Long Axis Orientation
$x(k_{\max})$	10, 7, 7	(-0.5,-0.5, 0.7071)
$x(k_{\min})$	7.37, 5.16, 5.16	(-0.5,0.5, 0.7071)

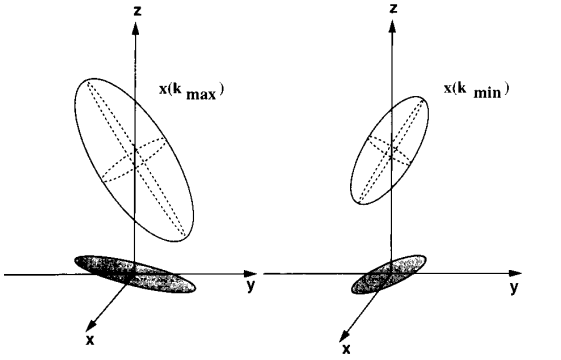

Fig. 6. The ellipsoids used for the angle sensitivity analysis. The shadows are shown to emphasize the orientation of the ellipsoid.

then the outcome is uncertain. For lower signal-to-noise ratios, the results indicate that the performance of the model identifier deteriorates and the transition region widens. As expected, outside of these relatively narrow transition regions, the model identifier chooses the hypothesized model which more closely approximates the true ellipsoid dynamics and, in particular, more closely matches the true ejection fraction. These results show that, even for low ISNR, the model identifier based on simple hypothesized models will adequately capture dynamics reflecting our quantity of interest, i.e., the ejection fraction.

B. Dynamic Model Mismatch

Next, we evaluate the error introduced by dynamic model mismatch and investigate methods to minimize the error by introducing a process noise term in our smoothing filter reconstruction, as discussed in Section II-B. A computer simulated 3-D ellipsoid and its noisy measurements are generated as described in (7) and (8). The initial ellipsoid, true projection geometry, and smoothing filter initialization are exactly as described in Section III-A. The true dynamics include periodic contraction/expansion without rotation as described by (17) with $c_t = 0.9615$ and $\theta_t = 0$ which yields an ejection fraction $\mathrm{EF}_t = 0.60$. A smoothing filter based on the RTS smoothing algorithm is implemented to reconstruct the 3-D ellipsoid from the noisy 2-D projections. This smoothing filter is based on the periodic dynamic model given by matrices $A_m(k)$ of the form (17) with modeled contraction and rotation rates c_m and θ_m. In reality, a method such as model identification might have been used to choose these matrices $A_m(k)$. For the experiment, these model dynamics consist of simple periodic contraction/expansion with no rotation chosen to yield a corresponding intrinsic ejection fraction of $\mathrm{EF}_m = 0.70$, which corresponds to $c_m = 0.9515$. An estimated ejection fraction value is calculated from the reconstructed ellipsoids as q and ISNR vary.

The results of this simulation are given in Fig. 5, which shows the variation of the percent error in the ejection fraction estimate with q. This percent ejection fraction error is defined as

$$\mathrm{EF\ Error}(\%) = \frac{|\mathrm{True\ EF} - \mathrm{Estimated\ EF}|}{\mathrm{True\ EF}} \times 100. \quad (21)$$

Note that the percent ejection fraction error is flat for a wide range of q even at high levels of measurement noise. At the highest noise level, it is possible to reduce the percent ejection fraction error by a factor of two by appropriate choice of q. Thus, q may be effectively used to minimize the error introduced by dynamic model mismatch by varying the amount of smoothing introduced by the filter, though we do not in fact bother to do this in our use of real data to follow.

C. Projection Geometry—A Sensitivity Analysis

Finally, we investigate the sensitivity of the 3- and 2-D data processing approaches (described in Section II-B) as the true projection geometry is varied. Both of these data processing approaches are based on an assumed projection geometry also described in Section II-B. In this section, we investigate the error in the ejection fraction estimate introduced by the assumed projection geometries underlying both the 3- and 2-D processing of the projection data.

The experimental procedure used for this sensitivity analysis is as follows. We generate computer-simulated dynamically evolving ellipsoids whose observations are taken as *noiseless* projections at a range of true projection geometries. For each of these true projection geometries, the noiseless observations are processed using both the 3- and 2-D assumed geometries. Static reconstruction is used to eliminate the uncertainty due to imperfectly known dynamics. The ejection fraction estimate is formulated for both methods and compared to the true ejection fraction.

The computer-simulated ellipsoids are illustrated in Fig. 6. The parameters for these ellipsoids are chosen so that our experiment is a *worst case* sensitivity analysis in the *physiological* sense. That is, a real left ventricle is expected to be much less eccentric than the ellipsoids being considered

here; the real left ventricular dynamics are expected to display only a slight rotation instead of the gross rotation used here. The dynamics that relate the fully expanded ellipsoid and fully contracted ellipsoids ($x(k_{\max})$ and $x(k_{\min})$) consist of an isotropic scaling by 0.7368 and a rotation of 90° about the z-axis, yielding an ejection fraction of 0.60.

The range of true projection geometries, which are used to generate the data (projections of the ellipsoid), consist of three projection planes which we denote $\{C_{t1}, C_{t2}, C_{t3}\}$. The first two are given by the (orthogonal) xz- and yz-planes. The third plane is specified by (13) or equivalently by (14)–(16) with $\Phi = 45°$ and $0° < \Theta < 90°$, which captures our prior belief that, in a real acquisition, the LAO image plane contains the greatest amount of variability.

For the 3-D processing approach, the three views are processed together as a single reconstruction problem. Here, we assume a projection geometry described in Section II-B and represented by the set of matrices $\{C_{m1}, C_{m2}, C_{m3}\}$ (as in (14)–(16) with $\Phi = \Theta = 45°$) or equivalently $\tilde{C}_m$ (as described in Section II-A). Because the observations are noiseless, a static reconstruction method is used which gives $\hat{x}(k) = (\tilde{C}_m^T \tilde{C}_m)^{-1} \tilde{C}_m^T y(k)$ where $y(k)$ are the observations of the ellipsoid. From the reconstructed ellipsoids $\hat{x}(k_{\max})$ and $\hat{x}(k_{\min})$, the estimated ejection fraction is calculated using (1).

For the 2-D processing approach, each view is processed individually. That is, the areas of the projections of $x(k_{\max})$ and $x(k_{\min})$ in each view are used to calculate the 2-D ejection fraction of that view. Then, the three 2-D ejection fractions are combined using (9) to obtain a 3-D ejection fraction estimate.

The percent ejection fraction errors from this angle sensitivity analysis are presented in Fig. 7. For the 3-D processing, the results show that, for a wide range of true projection geometries, the error in the ejection fraction estimate is small, less than 10%. While not as impressive as the 3-D results, the 2-D results show that the ejection fraction errors are less than 12% for a wide range of true projection geometries. Since this analysis is a worst case study, in general, the 2-D processing will be less affected by variations than is indicated in Fig. 7.

IV. Application to Real Data

In this section, our approach will be applied real data. Note, once again, that these approaches require as their inputs ellipses that have been extracted from the myocardial perfusion images via a preprocessing step. For this work, a very simple ellipse extraction routine is used (see [20] for details) and the measurement noise variance is assumed to be $R = rI$ where r is chosen empirically.

In addition, the outputs of the model identifier and smoothing filter are affected by the variance of the process noise, Q, assumed to be qI. It would also be logical to use a value of q that is in the range that minimizes the effect of residual dynamic model mismatch for the given r, as was illustrated in Section III. However, for this work, we use an empirically chosen value for q.[3] Specific values for the parameters r, q used for each case are given in the respective section discussing that case.

[3] An alternative to these empirically chosen values for the parameters r, q, which control smoothing, is discussed in [21].

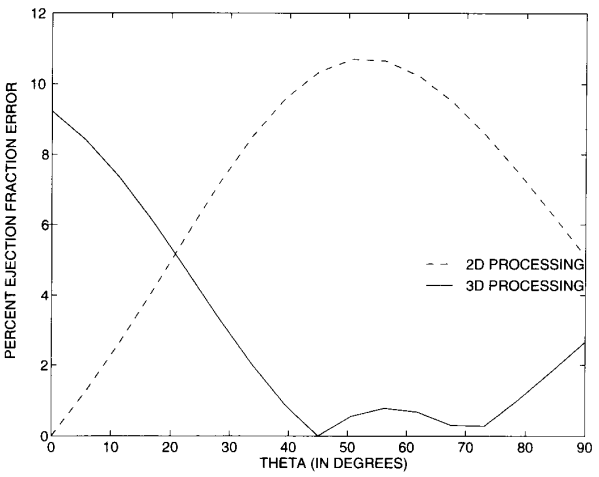

Fig. 7. Worst case angle sensitivity analysis results.

The ejection fraction calculated from myocardial perfusion images using our methods is compared to a "gold standard" (GS) ejection fraction obtained using MUGA images. Thus, the ejection fraction estimate based on myocardial perfusion images is evaluated by calculating the sample correlation,[4] $\rho_s(x, y)$, with the GS value.

A. 2-D Processing

In 2-D processing of the data, each view is processed individually. That is, a model identification scheme is applied to each view to determine which of three hypothesized models best approximates the true ellipse dynamics. Next, the model chosen by a simple vote of the outputs of the model identifier for the three views is used in a Rauch-Tung-Striebel smoothing filter to reconstruct the underlying ellipses. From the reconstructed ellipses, an effective 2-D ejection fraction for each view is found. Then, using the formula given in (9), an estimate of the 3-D ejection fraction is calculated.

The model identification scheme is implemented in the following way. For each of the three views, the input to the model identifier consists of the set of 16 ellipses extracted from the raw data for that view. The observations are of the ellipses themselves; therefore, the matrix C that specifies the projection geometry in (8) given by the identity. Three hypothesized models are used which yield hypothesized ejection fractions $\mathrm{EF}_1 = 0.60$, $\mathrm{EF}_2 = 0.40$, and $\mathrm{EF}_3 = 0.20$, respectively. The specific dynamics used for each of these hypothesized models are of the form of (17), where the parameters c_m are chosen so that the time (i.e., frame) of maximal contraction matches the corresponding time determined by eye from the data (i.e., so end systole of the model matches end systole of the heart data). Once again, the model identifier is initialized as in (18) and (19). The measurement noise variance r is chosen empirically

[4] Here, sample correlation coefficient is given as $\rho_s(x, y) = \frac{\mathrm{cov}_s(x,y)}{\sigma_{s,x}\sigma_{s,y}}$ where $\mathrm{cov}_s(x, y)$ refers to the sample covariance of x and y and $\sigma_{s,x}$ and $\sigma_{s,y}$ are the sample standard deviations of x and y, respectively [22].

to be 100. The value of q is set to zero to accentuate the difference between the three models. The dynamic model used for the smoothing phase is then chosen by a simple vote of the individual decisions of the model identifier for the three views.

Next, the Rauch-Tung-Striebel smoothing filter for each view is implemented based on the dynamic model chosen by the model identifier phase. For the smoothing filter, the empirically chosen values of r/q is 2. Again, the initialization of the smoothing filter is as given in (18) and (19). The 3-D ejection fraction estimate for each individual is obtained from the effective 2-D ejection fraction estimates using (9). Each 2-D ejection fraction is obtained using (1) (with volumes replaced by areas).

We begin by comparing the 2-D based estimated ejection fraction values to the GS ejection fraction values for each of 14 patients. For the data presented in Fig. 8(a), the sample correlation coefficient is calculated to be $\rho_s = 0.9135$. In addition, the 95% confidence region [23] is given as $0.7431 < \rho < 0.9727$. These results can be compared to the traditional "static" estimate of ejection fraction which is calculated using only the ES and ED frames of the raw (unsmoothed) data. Ellipses are extracted from the ES and ED frames and the 3-D ejection fraction estimate is calculated using (9). The correlation coefficient for this scenario is 0.7532. Thus, the RTS-based ejection fraction estimate is more robust to noise in spite of the simplified assumed dynamics.

B. 3-D Processing

In this section, model identification and smoothing filter reconstruction are applied to directly combine the set of 2-D observations as projections of a single 3-D ellipsoid that approximates the left ventricle. Based on the reconstructed dynamically evolving ellipsoid, an estimate of the ejection fraction is calculated. For this processing, an assumed projection geometry is used in which ANT and LAT views correspond to projections onto orthogonal planes and the LAO view corresponds to a projection onto a plane that is tilted by $\pi/4$ from the plane that is orthogonal to both the ANT and LAT planes, as discussed in Section II-B and shown in Fig. 2. The normal to this modeled LAO plane is given as in (13) with $\Theta = \Phi = 45°$.

The model identifier processes the combined data set from all three views for each individual to determine which of the hypothesized models should be used to model the true dynamics in the smoothing filter-based reconstruction stage. The hypothesized models and filter initializations are analogous to those described in Section IV-A. The values of r and q are chosen to be 100 and zero, respectively. The Rauch-Tung-Striebel smoothing filter then uses the dynamic model chosen by the model identifier together with $r/q = 2$. The 3-D ejection fraction estimate for each individual is then obtained from the volume change of these ellipsoids using (1).

Fig. 8(b) compares the GS ejection fraction values and the ejection fraction estimates based on the 3-D dynamic approach. The sample correlation coefficient is calculated to be $\rho_s = 0.8527$ with a 95% confidence interval of $0.5883 < \rho < 0.9524$. Again, these results can be compared to the "static" ejection fraction estimate which is based on only ellipses extracted from the ES and ED frames of the unsmoothed data and the same assumed projection geometry. For this scenario, $\rho_s = 0.6981$ which again demonstrates the robustness introduced by the RTS-smoothing.

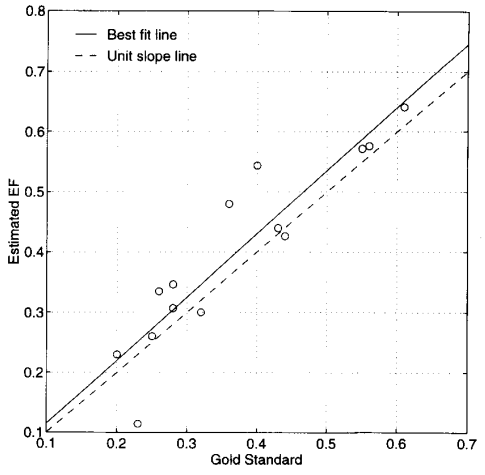

(a)

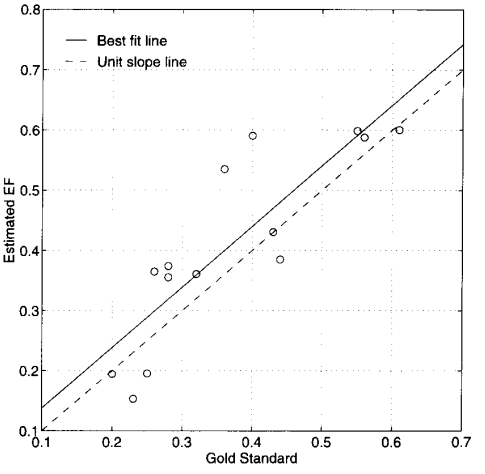

(b)

Fig. 8. Comparison of GS and EF estimates for 14 patients. (a) GS versus 2-D based EF estimates. (b) GS versus 3-D based EF estimates.

These results indicate that the 3-D processing did not perform as well as the 2-D processing, which seems counterintuitive. One explanation is that, in the 3-D processing, the interaction between the imperfectly known dynamics and the imperfectly known projection geometry may result in this greater error. In contrast, for the 2-D processing, the dynamics and projection geometry are handled independently. Further study with a larger sample size will be needed to fully understand this phenomenon.

V. Conclusion

This paper has outlined a model-based statistical approach to obtain a dynamic estimate of left ventricular ejection fraction

from a gated set of planar myocardial perfusion images. This approach was tested on simulated as well as real myocardial perfusion data. Although a relatively small sample size was used, the smoothing filter-based ejection fraction estimates showed a high degree of correlation with the GS ejection fraction estimates.

Further studies might directly apply our dynamically based smoothing techniques to other imaging modalities (e.g., MUGA) to obtain ejection fraction estimates. In addition, more hypothesized models may be included in the model identification phase so that the assumed ejection fraction used in the smoothing filter-based reconstruction is closer to the true ejection fraction. Finally, a circular smoothing algorithm might be considered which incorporates the additional constraint that the ellipsoid estimate at initial and final points of the cardiac cycle should be the same; thus, capturing a true periodicity assumption on the cardiac dynamics.

ACKNOWLEDGMENT

The authors would like to thank Dr. C. Boucher and Dr. D. Chesler who provided the myocardial perfusion images used in this work.

REFERENCES

[1] Y. Bresler, J. A. Fessler, and A. Macovski, "Model-based estimation techniques for 3-D reconstruction from projections," *Machine Vision Applicat.*, vol. 1, pp. 115–126, 1988.

[2] Y. Bresler and A. Macovski, "Three-dimensional reconstruction from projections with incomplete and noisy data by object estimation," *IEEE Trans. Acoust., Speech, Signal Processing*, vol. ASSP-35, 1987.

[3] W. C. Karl, G. C. Verghese, and A. S. Willsky, "Reconstructing ellipsoids from projections," *CVGIP: Graphical Models Image Processing*, vol. 56, no. 2, pp. 124–129, 1994.

[4] J. L. Prince, "Geometric model-based estimation from projections," Ph.D. dissertation, Massachusetts Institute of Technology, Jan. 1988.

[5] D. J. Rossi and A. S. Willsky, "Reconstruction from projections based on detection and estimation of objects—Parts I and II: Performance analysis and robustness analysis," *IEEE Trans. Acoust., Speech, Signal Processing*, vol. ASSP-32, no. 4, pp. 886–906, 1984.

[6] C. A. Boucher, "Detection and location of myocardial infarction using technetium-99 m sestamibi imaging at rest," *Amer. J. Cardiol.*, vol. 66, pp. 32E–35E, Oct. 1990.

[7] J. Heo *et al.*, "New myocardial perfusion imaging agents: Description and applications," *Amer. Heart J.*, pp. 1111–1117, May 1988.

[8] A. Sinusas *et al.*, "Quantitative planar imaging with technetium-99 m methoxyisobutyl isonitrile: Comparison of uptake patterns with thallium-201," *J. Nucl. Med.*, pp. 1456–1463, 1989.

[9] S. R. Underwood *et al.*, "Left ventricular volume and ejection fraction determined by gated blood pool emission tomography," *Brit. Heart J.*, vol. 53, pp. 216–222, 1985.

[10] R. H. Eich, *Introduction to Cardiology*. New York: Harper & Row, 1980.

[11] I. Mirsky, D. Ghista, and H. Sandler, *Cardiac Mechanics: Physiological, Clinical, and Mathematical Considerations*. New York: Wiley, 1974.

[12] E. Goldberger, *Essentials of Clinical Cardiology*. Philadelphia: Lippincott, 1990.

[13] A. Gelb, Ed., *Applied Optimal Estimation*. Cambridge, MA: MIT Press, 1988.

[14] A. Buda and E. Delp, "Digital two-dimensional echocardiography," in *Digital Cardiac Imaging*. New York: Martinus Nijhoff, 1985, ch. 11.

[15] A. Aisen and A. Buda, "Magnetic resonance imaging of the heart," in *Digital Cardiac Imaging*, A. Buda and E. Delp, Eds. New York: Martinus Nijhoff, 1985, ch. 15.

[16] M. H. Davis, B. Rezaie, and F. L. Weiland, "Assessment of left ventricular ejection fraction from technitium-99m-methoxy isobutyl isonitrile multiple-gated radionuclide angiocardiography," *IEEE Trans. Med. Imag.*, vol. 12, pp. 189–199, June 1993.

[17] R. Chan and W.-C. Siu, "Fast detection of ellipses using chord bisectors," in *IEEE ICASSP*, pp. 2201–2204, 1990.

[18] J. Porrill, "Fitting ellipses and predicted confidence envelopes using a bias corrected Kalman filter," *Image Vision Computing*, vol. 8, pp. 37–41, Feb. 1990.

[19] H. K. Yuen, J. Illingworth, and J. Kittler, "Detecting partially occluded ellipses using the Hough transform," *Image Vision Computing*, vol. 7, pp. 31–37, Feb. 1989.

[20] S. Jaggi, "Estimation of dynamically evolving ellipsoids with applications to cardiac imaging," M.S. thesis, Massachusetts Institute of Technology, Sept. 1992.

[21] J. A. Fessler, "Nonparametric fixed-interval smoothing with vector splines," *IEEE Trans. Signal Processing*, vol. 39, pp. 852–859, Apr. 1991.

[22] R. Anderson and T. Bancroft, *Statistical Theory in Research*. New York: McGraw-Hill, 1952.

[23] H. D. Brunk, *An Introduction to Mathematical Statistics*. New York: Xerox College, 1975.

[24] J. Juni and A. Buda, "Radionuclide imaging of the heart," in *Digital Cardiac Imaging*, A. Buda and E. Delp, Eds. New York: Martinus Nijhoff, 1985, ch. 13.

[25] L. Opie, *The Heart*. New York: Grune & Stratton, 1984.

[26] G. Strang, *Linear Algebra and Its Applications*. New York: Harcourt, Brace, Jovanovich, 1988.

[27] E. Jacobs, *Medical Imaging: A Concise Textbook*. Tokyo: Igaku-Shoin, 1987.

[28] I. Meschan and D. Ott, *Introduction to Diagnostic Imaging*. Philadelphia: Saunders, 1984.